



**HAL**  
open science

## Application of the Adler-Lane-Steele model to porous $\text{La}_2\text{NiO}_{4+d}$ SOFC cathode: influence of interfaces with gadolinia doped ceria

Aurélien Flura, Clément Nicollet, Vaibhav Vibhu, Bernhard Zeitmetz, Aline Rougier, Jean-Marc. Bassat, Jean-Claude Grenier

► **To cite this version:**

Aurélien Flura, Clément Nicollet, Vaibhav Vibhu, Bernhard Zeitmetz, Aline Rougier, et al.. Application of the Adler-Lane-Steele model to porous  $\text{La}_2\text{NiO}_{4+d}$  SOFC cathode: influence of interfaces with gadolinia doped ceria. *Journal of The Electrochemical Society*, 2016, 163 (6), pp.F523-F532. 10.1149/2.0891606jes . hal-01301743

**HAL Id: hal-01301743**

**<https://hal.science/hal-01301743>**

Submitted on 21 Jan 2021

**HAL** is a multi-disciplinary open access archive for the deposit and dissemination of scientific research documents, whether they are published or not. The documents may come from teaching and research institutions in France or abroad, or from public or private research centers.

L'archive ouverte pluridisciplinaire **HAL**, est destinée au dépôt et à la diffusion de documents scientifiques de niveau recherche, publiés ou non, émanant des établissements d'enseignement et de recherche français ou étrangers, des laboratoires publics ou privés.

# Application of the Adler-Lane-Steele Model to Porous $\text{La}_2\text{NiO}_{4+\delta}$ SOFC Cathode: Influence of Interfaces with Gadolinia Doped Ceria

A. Flura, C. Nicollet, V. Vibhu, B. Zeimetz, A. Rougier, J.-M. Bassat, and J.-C. Grenier<sup>‡</sup>

ICMCB, CNRS, Université de Bordeaux, 33608 PESSAC, France

Electrochemical impedance spectroscopy measurements carried out on  $\text{La}_2\text{NiO}_{4+\delta}$ (LNO)// $\text{Ce}_{0.8}\text{Gd}_{0.2}\text{O}_{2-\delta}$ (GDC)//3mol.%  $\text{Y}_2\text{O}_3$ - $\text{ZrO}_2$ (TZ3Y) half-cells from 500°C to 800°C revealed that the impedance of the LNO electrode is Gerischer-like. Based on experimental data of the porosity, tortuosity, surface area, molar volume and thermodynamic factor of the LNO electrode sintered at 1200°C, the ionic conductivity  $\sigma_{i(\text{LNO})}$  and the surface exchange coefficient  $\mathfrak{N}_0$  of the LNO electrode are calculated using the Adler-Lane-Steele (ALS) model. Surprisingly, the polarization resistance of the half-cell is shown to depend on the sintering temperature of the GDC interlayer, which is varied from 1200°C up to 1450°C. Whatever the sintering conditions of GDC, the calculated  $\mathfrak{N}_0$  values agree with those obtained by recently published pulse isotopic exchange (PIE) experiments. Indeed, the oxygen reduction reaction mostly occurs at the LNO grain surface. However, the calculated ionic conductivity of the electrode vary depending on the GDC sintering temperature. X-ray diffraction studies of the LNO//GDC and GDC//TZ3Y interfaces reveal that cations interdiffusion occurs in both cases. The interfacial GDC layer may act as a bottleneck for the oxide ion transfer from the LNO electrode toward the TZ3Y electrolyte, and *vice-versa*, resulting in an increase of the series and polarization

In the last decade, the lanthanide nickelates have attracted more and more attention due to their good performances as cathode materials for solid oxide fuel cells, mainly with regard to their intrinsic mixed ionic electronic conducting (MIEC) properties.<sup>1-3</sup> For instance, Bassat et al.<sup>4</sup> and Burriel et al.<sup>5</sup> showed  $\text{La}_2\text{NiO}_{4+\delta}$  (namely LNO) to exhibit high values of surface exchange and diffusion coefficients ( $k^*$  and  $D^*$ ). In addition, LNO is chemically stable in the range of  $p\text{O}_2 = 1 - 5 \cdot 10^{-5}$  atm, from room temperature up to 1300°C.<sup>6</sup> However, the polarization resistance values reported in the literature are rather high: for instance, Hildenbrand et al.<sup>7</sup> obtained an optimum value  $R_p \approx 850 \text{ m}\Omega \cdot \text{cm}^2$  at 600°C, for the following half-cell:  $\text{La}_2\text{NiO}_{4+\delta}(\text{porous})//\text{La}_2\text{NiO}_{4+\delta}(\text{dense})//\text{Ce}_{0.8}\text{Y}_{0.2}\text{O}_{2-\delta}/3\text{mol.}\% \text{ Y}_2\text{O}_3\text{-ZrO}_2$ . These authors strove to understand the mechanism of the oxygen electrode reaction (OER) of  $\text{La}_2\text{NiO}_{4+\delta}$ <sup>7</sup> using the Adler-Lane-Steele (ALS) model.<sup>8</sup> With respect to the significant  $\text{O}^{2-}$  solid-state diffusion anisotropy in the LNO bulk material, they proposed that surface diffusion of the oxygen species should play a major role in the oxygen reduction reaction.

In this paper, the OER has been studied for  $\text{La}_2\text{NiO}_{4+\delta}$  electrode deposited on a 3 mol. %  $\text{Y}_2\text{O}_3$ - $\text{ZrO}_2$  (TZ3Y) dense electrolyte, covered with a barrier layer made of  $\text{Ce}_{0.8}\text{Gd}_{0.2}\text{O}_{2-\delta}$  (GDC), in order to avoid the formation of the detrimental  $\text{La}_2\text{Zr}_2\text{O}_7$  pyrochlore interphase.<sup>9,10</sup>

The aim of this study is firstly to support that the ALS model can be applied to LNO//GDC//TZ3Y designed half-cells. Secondly, the influence on the electrochemical performances of the interface between the GDC interlayer and the LNO porous electrode will be pointed out.

## Experimental

**Preparation of cell components.**—The TZ3Y dense electrolyte membrane ( $\approx 90 \mu\text{m}$ ) was kindly provided by Indec company. Commercial sub-micronic powders,  $\text{La}_2\text{NiO}_{4+\delta}$  from Marion Technologies Co. and  $\text{Ce}_{0.8}\text{Gd}_{0.2}\text{O}_{1.90}$  from Rhodia Co., were respectively used as starting materials for preparing the electrode, and the interfacial barrier layer between LNO and TZ3Y.

$\text{La}_2\text{NiO}_{4+\delta}$ //GDC//TZ3Y symmetrical half-cells were made as follows: GDC interface layers were screen-printed on both sides of the TZ3Y electrolyte, and sintered at various temperatures between 1200°C and 1450°C, for 3 h, in air with a controlled heating rate of 2°C/min, resulting in a layer thickness of approximately 2  $\mu\text{m}$ . Subsequently,  $\text{La}_2\text{NiO}_{4+\delta}$  ink was screen-printed on top of the GDC

interface layer, and sintered at 1200°C, for 1 h, in air, with a heating rate of 2°C/min, leading to cathode layers of about 20  $\mu\text{m}$  thick.

A collecting layer of  $\text{LaNi}_{0.6}\text{Fe}_{0.4}\text{O}_3$  (LNF) was screen printed on both sides of the sintered LNO//GDC//TZ3Y half-cell. It was in situ sintered in the EIS setup at 900°C for 2h, allowing decreasing the overall series resistance of the cell during the EIS measurements. It was experimentally checked that this layer does not take part in the oxygen electrode reaction (OER).<sup>11</sup>

**Structural and microstructural characterizations of the materials.**—The powders were characterized by X-Ray diffraction (XRD) at room temperature using a PANalytical X'pert MPD diffractometer with  $\text{Cu-K}\alpha$  incident radiation.

The X-ray diffractograms were fitted by profile matching using the Fullprof software.<sup>12</sup>

SEM observations of the cross-section of LNF// $\text{La}_2\text{NiO}_{4+\delta}$ //GDC//TZ3Y half-cells were carried out using a JEOL JSM 6330F. Samples were prepared by embedding under vacuum the cell in an epoxy resin (EpoFix from Struers A/S, Denmark), then were mirror polished. The thickness, porosity and pore diameter of the electrode microstructure were determined by means of image analysis using the Image J software.

The specific surface area of LNO electrodes was determined using the B.E.T. method through nitrogen physisorption measurements carried out on a Quantachrome autosorb apparatus. To obtain enough powder ( $m_{\text{LNO}} \approx 350 \text{ mg}$ ), the LNO ink used for the LNF//LNO//GDC//TZ3Y half-cell preparation was sintered in an alumina crucible, using the same annealing treatment that the one used for the preparation of the half-cell. Pieces of LNO electrode were obtained and used for the determination of the specific surface area.

**Electrochemical impedance spectroscopy measurements.**—The electrochemical impedance spectroscopy (EIS) measurements were performed in the setup depicted in Fig. 1. Impedance measurements of the LNF//LNO//GDC//TZ3Y symmetrical half-cells were carried out in the range  $10^6 \text{ Hz} - 10^{-1} \text{ Hz}$ , using an Autolab PGStat 308 frequency response analyzer, the *ac* amplitude being fixed at 50 mV. Gold grids were used as current collectors. Data were fitted using two softwares: Zview (Scribner Associates) and the home-made CANELEIS.<sup>13</sup> The latter was used more specifically to perform Kramers-Kronig test.<sup>14</sup> The electrochemical experiments were performed at decreasing temperature, from 800°C down to 500°C, in air, at  $i_{\text{dc}} = 0\text{A}$ .

<sup>‡</sup>E-mail: jean-claude.grenier@icmcb.cnrs.fr

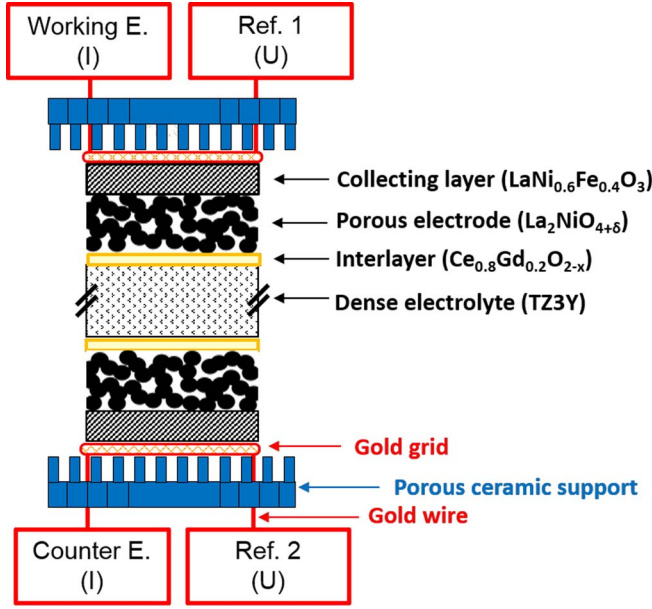


Figure 1. EIS measurement setup.

## Results and Discussion

**The Adler-Lane-Steel model.**—Linear *ac* polarization behavior of the  $\text{La}_2\text{NiO}_{4+\delta}$  MIEC electrode was studied considering the ALS model<sup>8</sup> which “uses continuum modeling to analyze the mechanism of the oxygen reduction reaction at a porous mixed-conducting oxygen electrode”. The model describes the conversion of the electronic current into ionic current over the whole thickness of the electrode. At zero-bias, the impedance  $Z$  of a symmetrical cell is:

$$Z = R_{\text{electrolyte}} + Z_{\text{interfaces}} + Z_{\text{chem}} \quad [1]$$

$R_{\text{electrolyte}}$  is related to the  $\text{O}^{2-}$  ionic solid-state transport in the electrolyte,  $Z_{\text{interfaces}}$  describes the electron transfer at the current collector/electrode interface and the  $\text{O}^{2-}$  diffusion at the electrode/electrolyte interface, and  $Z_{\text{chem}}$  is a convoluted impedance including the following reaction steps *i*) the solid-state diffusion of oxygen electro-active species in the electrode, *ii*) the oxygen surface exchange between the electrode and its surrounding atmosphere and *iii*) the diffusion of molecular  $\text{O}_2$  in this atmosphere.<sup>15</sup> Within the limit where only steps *i*) and *ii*) co-limit the oxygen reduction reaction,  $Z_{\text{chem}}$  reduces to Eq. 2:<sup>16</sup>

$$Z_{\text{chem}} = R_{\text{chem}} \sqrt{\frac{1}{1 + j\omega (R_{\text{chem}} C_{\text{diff}})}} = R_{\text{chem}} \sqrt{\frac{1}{1 + j\omega (t_{\text{chem}})}} \quad [2]$$

In this case,  $Z_{\text{chem}}$  is mathematically equivalent to the Gerischer impedance.<sup>17,18</sup>  $R_{\text{chem}}$  and  $C_{\text{diff}}$  are the chemical resistance and capacitance reflecting co-limitation of the OER by the surface exchange coefficient  $\mathfrak{R}_{0(\text{MIEC})}$  and the ionic conductivity  $\sigma_{i(\text{MIEC})}$  of the MIEC;  $t_{\text{chem}}$  is the relaxation time of the Gerischer impedance. The expression of  $R_{\text{chem}}$ ,  $t_{\text{chem}}$  and  $C_{\text{diff}}$  have been defined by Adler et al.<sup>15</sup> through Eqs. 3, 4 and 5:

$$R_{\text{chem}} = \sqrt{\frac{RT}{2F^2} \times \frac{\tau}{(1 - \varepsilon) \cdot S_A \cdot \mathfrak{R}_{0(\text{MIEC})} \cdot \sigma_{i(\text{MIEC})}}} \quad [3]$$

$$t_{\text{chem}} = \frac{(1 - \varepsilon)}{V_m \cdot f_{\text{thermo}} \cdot S_A \cdot \mathfrak{R}_{0(\text{MIEC})}} \quad [4]$$

$$C_{\text{diff}} = \frac{t_{\text{chem}}}{R_{\text{chem}}} = \frac{F \cdot (1 - \varepsilon)^{1.5}}{f_{\text{thermo}} \cdot V_m} \times \sqrt{\frac{2 \cdot \sigma_{i(\text{MIEC})}}{RT \cdot \tau \cdot S_A \cdot \mathfrak{R}_{0(\text{MIEC})}}} \quad [5]$$

From these equations,  $\mathfrak{R}_{0(\text{MIEC})}$  and  $\sigma_{i(\text{MIEC})}$  can be determined from the Eqs. 6 and 7, respectively:

$$\mathfrak{R}_{0(\text{MIEC})} = \frac{(1 - \varepsilon)}{V_m \cdot f_{\text{thermo}} \cdot S_A \cdot t_{\text{chem}}} \quad [6]$$

$$\sigma_{i(\text{MIEC})} = \frac{RT}{2F^2} \times \frac{\tau \cdot V_m \cdot f_{\text{thermo}} \cdot t_{\text{chem}}}{((1 - \varepsilon) \cdot R_{\text{chem}})^2} \quad [7]$$

The key parameters used in these equations are the electrode porosity  $\varepsilon$ , the electrode tortuosity  $\tau$ , the molar volume of the MIEC material  $V_m$  and its surface area  $S_A$ .  $f_{\text{thermo}}$  is a thermodynamic factor related to the variation of the oxygen stoichiometry of the material upon change of the oxygen partial pressure.  $R_{\text{chem}}$  and  $t_{\text{chem}}$  are obtained via fitting the experimental impedance data using the Gerischer impedance. Finally,  $R$  and  $F$  have their usual meaning, the gas and Faraday constants,  $T$  being the temperature in K.

Another parameter which can be calculated using the ALS model is the thickness of the electrode involved in the oxygen electrode reaction, i.e. the diffusion length  $l_{\text{diff}}$ , which can be considered as the electrode active part. It is given by the Eq. 8:

$$l_{\text{diff}} = C_{\text{diff}} \times \frac{RT}{4F^2} \times \frac{V_m \cdot f_{\text{thermo}}}{(1 - \varepsilon)} = \sqrt{\frac{RT}{8F^2} \times \frac{(1 - \varepsilon) \cdot \sigma_{i(\text{MIEC})}}{\tau \cdot S_A \cdot \mathfrak{R}_{0(\text{MIEC})}}} \quad [8]$$

In order to use the ALS model, some important conditions must be fulfilled. Obviously, the first point is that the material should be a MIEC material – which is the case for  $\text{La}_2\text{NiO}_{4+\delta}$ . Secondly, the thickness of the electrode must be larger than the theoretical diffusion length as given by Eq. 8. Indeed, when the ORR is limited by the electrode thickness, a finite-length Gerischer impedance expression, as formulated by Boukamp et al.<sup>19</sup> for instance, should be considered. Thirdly, the Gerischer impedance resulting from the ALS model can only be applied to electrodes in which the limiting steps for the OER are the solid-state diffusion of  $\text{O}^{2-}$  and the oxygen exchange at the interface gas/electrode. Finally, the thickness of the electrode involved in the OER,  $l_{\text{diff}}$ , must be larger than the average diameter value of the electrode particles. Otherwise, a 3D model<sup>20</sup> should be considered, instead of the ALS model which is a 1D model.

**E.I.S. measurements of LNO porous electrodes.**—The impedance diagrams in the temperature range 500°C–800°C for symmetrical porous LNO electrodes sintered on a GDC/TZ3Y architecture are reported in Fig. 2. GDC is sintered at 1300°C for 3h, LNO at 1200°C for 1h. The series resistance  $R_s$  of the electrolyte has been subtracted from the impedance plot for the sake of clarity.

Three processes,  $P_1$ ,  $P_2$  and  $P_3$ , can be evidenced:  $P_1$  is clearly visible at high frequency ( $f \gg 10^4$  Hz) in Fig. 2a, for the diagrams obtained at 500–550°C, and is related to  $\text{O}^{2-}$  solid-state diffusion in the electrolyte materials (TZ3Y and GDC) with regards to previous works.<sup>21</sup> The low frequency intercept of  $P_1$  with the  $Z'$  axis is  $R_s$ .  $P_2$ , which exhibits a Gerischer impedance shape, is well depicted in Fig. 2b in the frequency range  $10^3$  Hz  $< f < 10^{-1}$  Hz for the diagrams measured at 600–700°C. This contribution is assigned to the oxygen electrode reaction occurring in the LNO electrode.  $P_3$  is clearly visible at low frequency ( $f < 10$  Hz) in Fig. 2c, for the diagrams obtained at 750°C and 800°C. This process is related to gas concentration phenomena occurring in the porous structure of the electrode and in the EIS setup.<sup>22,23</sup>

This paper is focused on the Gerischer impedance related to the LNO electrode. The accuracy of the diagram data was checked using the Kramers-Kronig (KK) relation<sup>24</sup> thanks to the CANELEIS software; a typical example is shown in Fig. 3.

Discrepancy appears between the KK plot and the experimental plot for  $f > 10^4$  Hz, i.e. for the process related to  $\text{O}^{2-}$  solid-state diffusion in the electrolyte materials. It is likely that overlapping with the impedance of the EIS setup wires is responsible for this behavior. At lower frequencies, the Gerischer impedance matches well with the KK plot, which is a guarantee of quality.

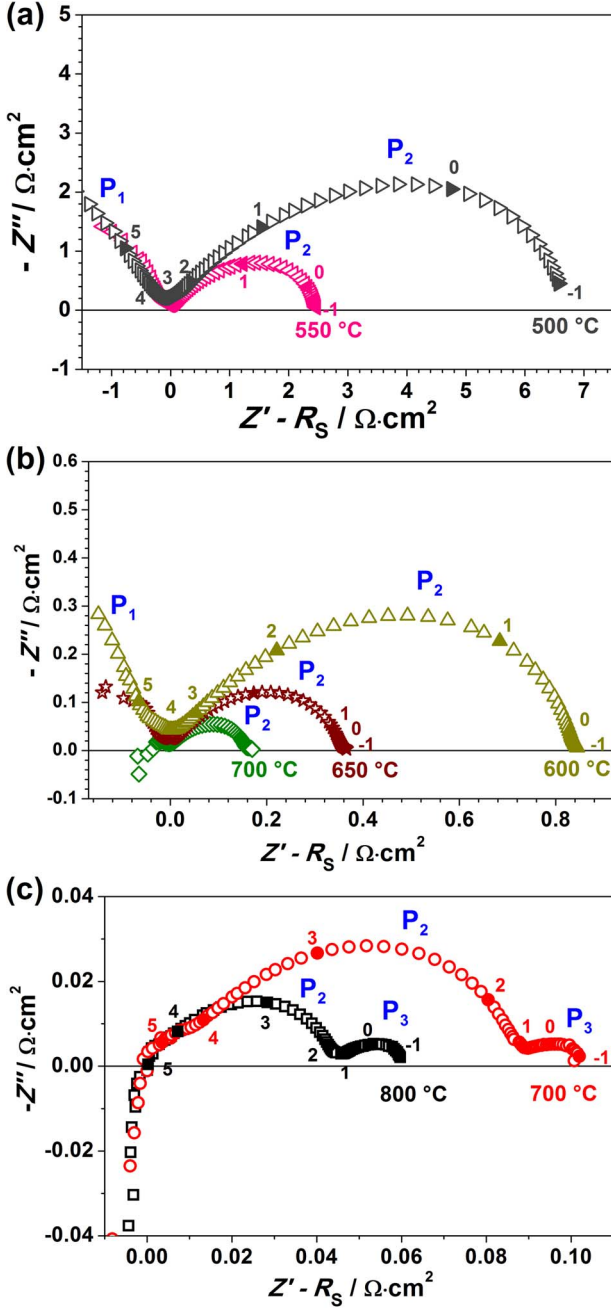


**Figure 2.** Typical impedance diagrams of a LNF//LNO//GDC//TZ3Y half-cell measured by EIS at various temperatures: GDC sintered at 1300°C for 3h, LNO sintered at 1200°C for 1h.

In order to obtain an optimal fit, a “fractal” expression of the Gerischer impedance was needed instead of the ideal case, as shown in Fig. 4. This fractal expression is given in Eq. 9 through the parameter  $\varphi$ . It allows a distribution of the relaxation time, as for a R//CPE element compared to a pure R//C process.

$$Z_{\text{chem}} = R_{\text{chem}} \sqrt[\varphi]{\frac{1}{1 + (j\omega(t_{\text{chem}}))^\varphi}} \quad [9]$$

The addition of a  $\text{LaNi}_{0.6}\text{Fe}_{0.4}\text{O}_3$  (LNF) collecting layer on top of the LNO porous electrode leads to an increase of  $\phi$  from 0.78 up to 0.94, but does not affect the polarization resistance value. As suggested in Refs. 25,26, it indicates that without an optimized collecting layer, non-uniform electronic current distribution occurs in the LNO

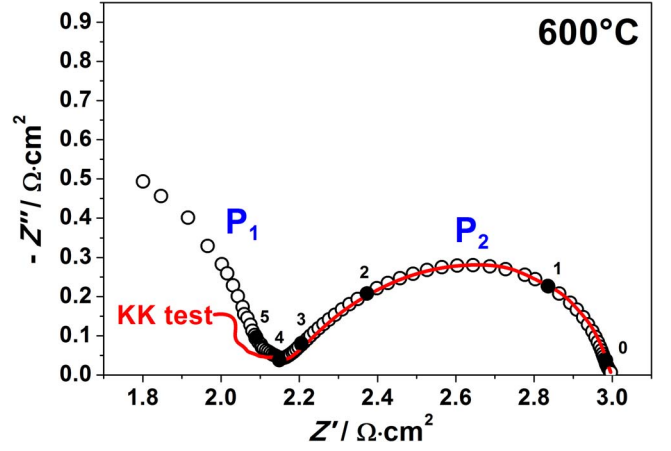


**Figure 3.** Kramers-Kronig (KK) test, carried out on the impedance diagram of the LNF//LNO//GDC//TZ3Y half-cell measured at 600°C.

electrode, which might be due to its porous structure, coupled with a high anisotropy of its electronic - and ionic - conduction.<sup>4</sup> Our results suggest that the value taken by  $\varphi$  increases with the uniformity of the current distribution. It is noteworthy that a value  $\varphi = 0.94$  is very close to the ideal Gerischer impedance ( $\varphi = 1$ ), as reported in Fig. 4.

Based on  $R_{\text{chem}}$  and  $t_{\text{chem}}$  parameters obtained from the Gerischer impedance data refinement,  $\Re_0$  and  $\sigma_{i(\text{LNO})}$  can be calculated using the Eqs. 6 and 7. However, at first, it was mandatory to determine parameters required for the ALS model, i.e. the thermodynamic factor  $f_{\text{thermo}}$ , the molar volume  $V_m$ , the specific surface area  $S_A$ , the porosity  $\varepsilon$  and the tortuosity  $\tau$  of the LNO porous electrode.

**Determination of the ALS model key parameters.—The thermodynamic factor.**—The thermodynamic factor<sup>27</sup> can be determined from TGA measurements carried out at various  $p\text{O}_2$ , then calculated using Eq. 10:

$$f_{\text{thermo}} = -\frac{1}{2} \frac{\partial \ln p(\text{O}_2)}{\partial \ln \delta} \quad [10]$$

From results reported in Ref. 6 for LNO, this factor has been calculated for temperatures ranging from 500 to 700°C; the results are reported in Fig. 5.

An almost straight line is obtained over the whole temperature range, with a value increasing from 240 to 296 between 500°C and

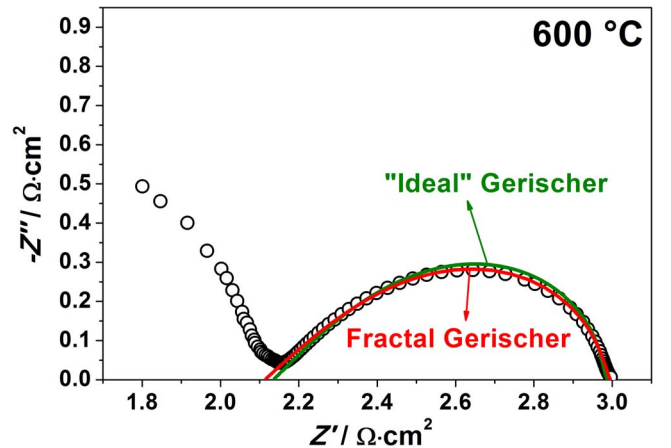


**Figure 4.** Impedance diagram of the LNF//LNO//GDC//TZ3Y half-cell measured at 600°C. The data are fitted using an “ideal” or fractal Gerischer impedance.

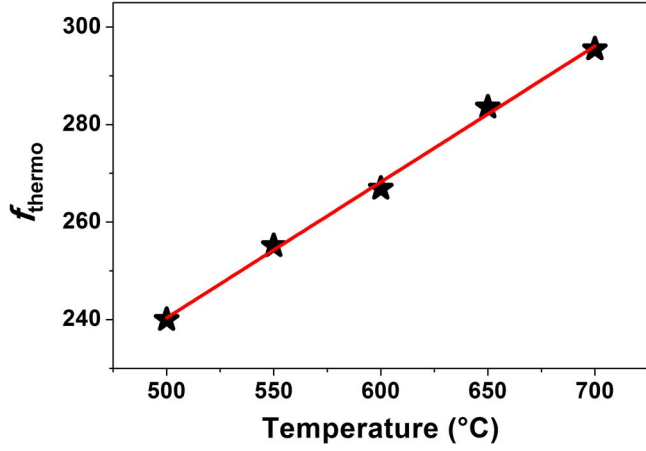


Figure 5. Thermal dependence of the thermodynamic factor of  $\text{La}_2\text{NiO}_{4+\delta}$ .

700°C. The linear regression of the data is given in Eq. 11:

$$f_{\text{thermo}} = 0.2787 \cdot T + 100.99 \quad [11]$$

with  $T$  in Celsius. The obtained values are somewhat smaller than those previously determined for  $\text{La}_2\text{Cu}_{0.5}\text{Ni}_{0.5}\text{O}_{4+\delta}$ ,<sup>27</sup> which denotes a higher capability of LNO to change its oxygen stoichiometry upon a variation of  $p\text{O}_2$ .

*The molar volume.*—The molar volume of LNO (Fig. 6) was calculated from the thermal variation of its lattice parameters determined in air, by in situ X-Ray Diffraction (XRD) measurements at decreasing temperature from 1400°C down to room temperature. Again, detailed data are given in Ref. 6.

From the linear regression of the molar volume data points,  $V_m$  can be calculated using Eq. 12:

$$V_m = 2.27 \times 10^{-3} \cdot T + 57.076 \quad [12]$$

with  $T$  in Celsius.

*The porosity.*—The porosity  $\epsilon$ , specific surface area  $S_A$  and tortuosity  $\tau$  of a porous LNO layer sintered at 1200°C on a GDC/TZ3Y electrolyte pellet were estimated from SEM micrographs. The microstructure of the electrode is shown in Fig. 7.

The porosity of the LNO electrode was determined as follows: at first, the "apparent density"  $\rho_{\text{app(LNO)}}$  of the porous LNO electrode was calculated from the parameters *i*)  $m_{\text{electrode}}$ , the weight of electrode material deposited on TZ3Y, *ii*)  $S_{\text{electrode}}$ , the electrode surface area,

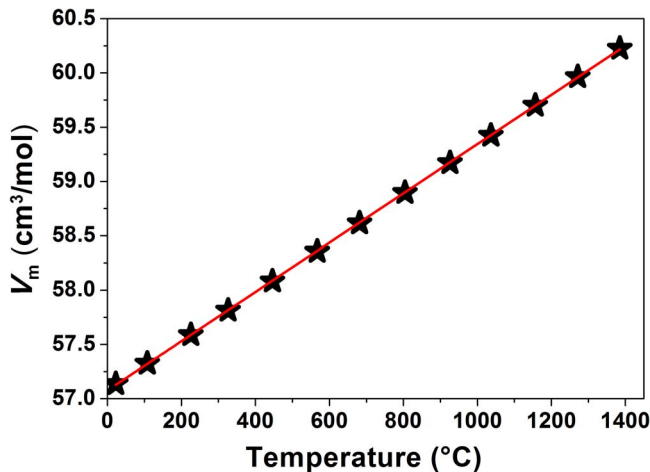


Figure 6. Thermal dependence of the molar volume  $V_m$  of  $\text{La}_2\text{NiO}_{4+\delta}$ .

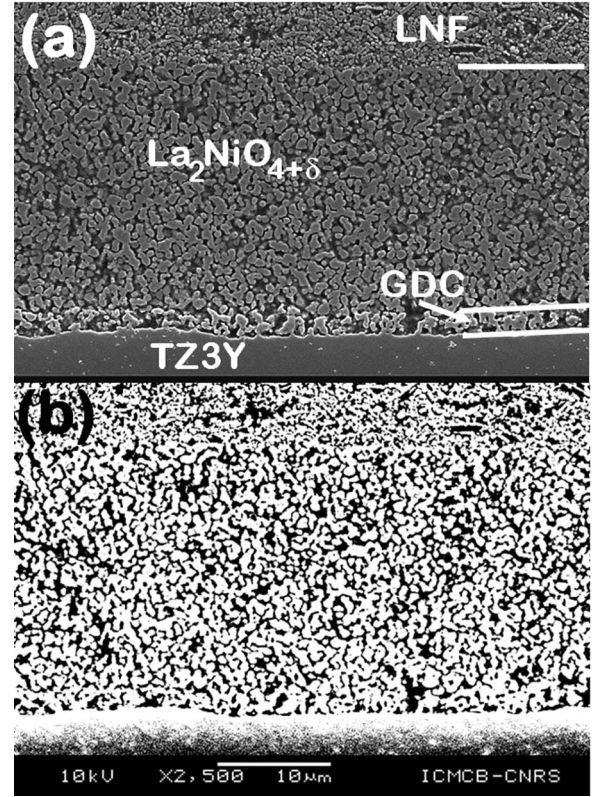


Figure 7. SEM images of the polished cross-section of the LNF/LNO/GDC/TZ3Y half-cell, LNO being sintered at 1200°C for 1h in air, GDC at 1300°C for 3 h. (a) Secondary electron image. (b) Image processed with Image J.

determined from a microscopy image of the electrode top surface using Image J software and *iii*)  $t_{\text{electrode}}$ , the average thickness of the electrode, measured from SEM micrographs. The apparent density takes into account the porosity of the electrode. It is calculated using Eq. 13:

$$\rho_{\text{app(LNO)}} = \frac{m_{\text{electrode}}}{S_{\text{electrode}} \times t_{\text{electrode}}} \quad [13]$$

Then, considering the theoretical density of LNO at room temperature  $\rho_{\text{theo(LNO)}} = 7.05 \text{ g/cm}^3$ , the porosity of the electrode is calculated using Eq. 14:

$$\epsilon = \frac{\rho_{\text{theo(LNO)}} - \rho_{\text{app(LNO)}}}{\rho_{\text{theo(LNO)}}} \quad [14]$$

The value obtained for the porosity is  $\epsilon \approx 0.36$ .

In addition, the value of the porosity was cross-checked by applying a threshold on the SEM image using Image J software (as shown in Fig. 7b), and calculating the black surface corresponding to the pores over the whole surface area ratio: a value of  $\epsilon \approx 0.35$  was determined. Based on these two results, a mean value of  $\epsilon \approx 0.35$  was used for the ALS model.

*The specific surface area.*—The specific surface area of the LNO electrode sintered at 1200°C was measured using two methods.

Firstly, it was determined from nitrogen physisorption measurements, using the B.E.T. method: the measured value was  $S_{\text{BET}} = 1.04 \text{ m}^2/\text{g}$ . As required by the ALS model, assuming a spherical particle size of  $0.55 \mu\text{m}$ , and taking into account the porosity of the electrode (35%) and the theoretical density, the value  $S_A = 48 \text{ 000 cm}^2/\text{cm}^3$  was calculated.

Secondly, the specific surface area of the electrode was estimated using the methodology proposed in reference 28, based on the average LNO particle diameter and the porosity of the electrode. Using Image

J software, the average diameter of the LNO particles was estimated from five different micrographs to be around  $0.55 \mu\text{m}$  after a sintering step at  $1200^\circ\text{C}$ , for 1h in air. For this methodology, the electrode is considered as a uniform array of identical cylindrical rods of radius  $R$ . In our case, it roughly simulates the interconnection between the LNO particles, which allows the  $\text{O}_2$  solid-state diffusion to occur. An estimation of the specific surface area  $S_A$  can then be obtained from Eq. 15:

$$S_A = \frac{2(1 - \varepsilon)}{R} \quad [15]$$

The radius of the rods was approximated to those of the LNO particles, i.e.  $R = 0.275 \mu\text{m}$ . Using  $\varepsilon \approx 0.35$ , a specific surface area  $S_A \approx 47\,000 \text{ cm}^2/\text{cm}^3$  was estimated, which is close from the value determined using the B.E.T. method.

For the subsequent model, the value  $S_A = 48000 \text{ cm}^2/\text{cm}^3$  obtained from the B.E.T. measurements was considered.

**The tortuosity.**—Determining the tortuosity of a porous electrode is a challenging point, since it normally requires specific techniques such as tomography<sup>29</sup> to be correctly achieved. However, an estimation of its value was done as discussed below.

The tortuosity  $\tau$  reflects the extra distance covered by an oxide ion to diffuse from a point of the electrode toward the electrolyte surface. With regards to the microstructure of the LNO electrode as shown in Fig. 7 and the porosity of the electrode  $\varepsilon \approx 0.35$ , it seems unlikely that the distance covered by  $\text{O}^{2-}$  will be larger than twice that of the straight line toward the electrolyte - but still, it should be higher than 1. Hence, it is expected for the tortuosity to range between 1 and 2. Based on a previous report in the literature for similar electrodes,<sup>29</sup> the tortuosity has been estimated at  $\tau = 1.5$ ; this value is used for further calculations.

#### Calculation of $\mathfrak{R}_0$ , $\sigma_{i(\text{LNO})}$ and $C_{\text{chem}}$ using the ALS model.—

$\mathfrak{R}_0$  and  $\sigma_{i(\text{LNO})}$  values were calculated from the impedance data Fig. 2, using Eqs. 6 and 7 of the ALS model. The calculated  $\text{O}_2$  surface exchange coefficient  $\mathfrak{R}_0$  was compared with values determined by Bouwmeester et al.,<sup>30</sup> using pulsed isotopic exchange (PIE) measurements on LNO powder.

The calculated  $\sigma_{i(\text{LNO})}$  was compared with the ionic conductivity of LNO determined by Boehm et al.<sup>4</sup> by isotopic exchange depth profiling of  $\text{O}_2$  (IEDP) measurements on dense LNO ceramic pellets. The thermal dependence of  $\mathfrak{R}_0$  and  $\sigma_{i(\text{LNO})}$  are shown in Fig. 8.

Over the whole temperature range, the values of the  $\text{O}_2$  surface exchange coefficient  $\mathfrak{R}_0$  calculated from the impedance data using the ALS model and those determined from PIE measurements show a perfect agreement, as well as the activation energies  $E_A \approx 1.50 \text{ eV}$  (Fig. 8a).

On the contrary, the calculated values of the ionic conductivity of LNO show some discrepancy as compared to those obtained from the IEDP experiments (Fig. 8b). The IEDP “ceramic” conductivity exhibits an activation energy  $E_A = 0.76 \text{ eV}$  at  $T < 600^\circ\text{C}$ , then  $E_A = 0.84 \text{ eV}$  above, close to the value  $E_A = 1.00 \text{ eV}$  obtained for the calculated ionic conductivity of LNO.

It is noteworthy that although the experimental  $\mathfrak{R}_0$  and  $\sigma_{i(\text{LNO})}$  plots originate from distinct studies and authors, both show that a slight change in the activation energy value occurs at around  $600^\circ\text{C}$ . This could be assigned to two different mechanisms of oxygen electrode reaction for LNO depending on the temperature range, but further studies would be needed to confirm this point.

The key fact of this preliminary study is that the  $\mathfrak{R}_0$  values calculated from the impedance data using the ALS model are consistent with the experimental  $\mathfrak{R}_0$  values published by Bouwmeester et al.,<sup>30</sup> which is quite satisfactory. For  $\sigma_{i(\text{LNO})}$ , if differences in the absolute values of the ALS plot compared to the experimental one are observed, their respective activation energy is close.

A possible explanation for this behavior is discussed in the following.

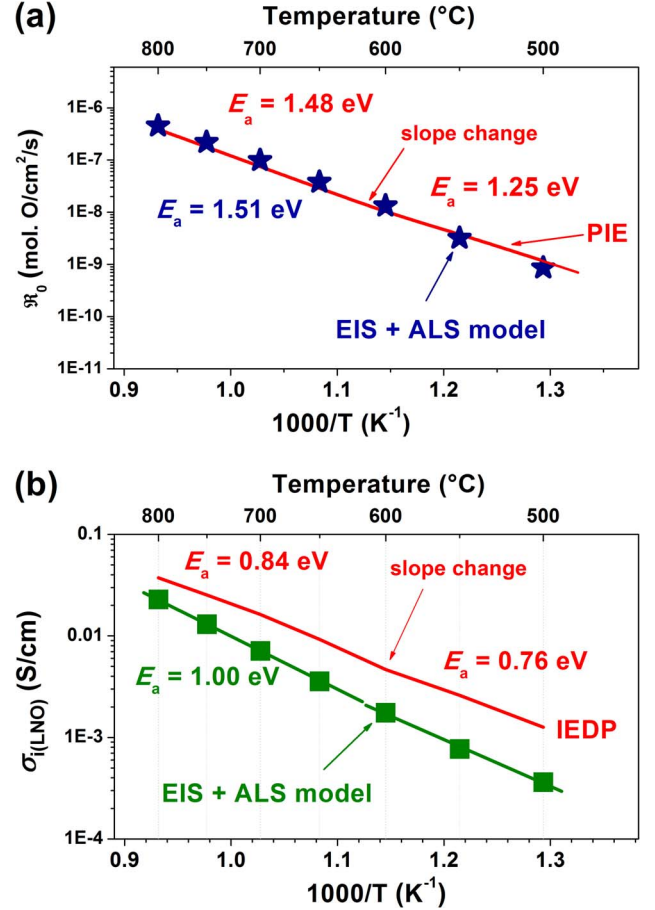


**Figure 8.** Thermal dependence of (a) the exchange surface coefficient  $\mathfrak{R}_0$  and (b) the ionic conductivity of LNO, calculated from EIS data using the ALS model. Comparison with PIE<sup>30</sup> and IEDP<sup>4</sup> data.

Using the experimental  $\mathfrak{R}_0$  and  $\sigma_{i(\text{LNO})}$  values from the literature, the ALS model predicts that a porous LNO electrode as prepared in this study should give at  $600^\circ\text{C}$  an optimal polarization resistance  $R_{\text{chem}} = 0.60 \Omega \cdot \text{cm}^2$ , for a relaxation time  $t_{\text{chem}} = 8.05 \cdot 10^{-2} \text{ s}$ . For our designed LNF//LNO//GDC//TZ3Y cell, a higher polarization resistance  $R_{\text{chem}} = 0.85 \Omega \cdot \text{cm}^2$  for  $t_{\text{chem}} = 6.3 \cdot 10^{-2} \text{ s}$  was obtained (cf. Fig. 3b), which indicates that the polarization resistance experimentally obtained is larger than the optimal calculated one.

Recent publications<sup>10,31–33</sup> have reported that reactivity occurs between LNO and GDC, for  $T > 700^\circ\text{C}$ . Results clearly indicate that mainly La, and Ni in a lesser extent, are able to diffuse in the GDC fluorite structure, which leads to the formation of a lanthanum doped GDC, and simultaneously to  $\text{La}_3\text{Ni}_2\text{O}_7$  at  $T > 1000^\circ\text{C}$ .<sup>10,32</sup> It is likely that the nature of the LNO//GDC interface has an impact on the EIS behavior. To verify this assumption, samples with GDC layer sintered at different temperatures were prepared.

#### Influence of the GDC interlayer on the oxygen electrode reaction impedance.—

To study the influence of the GDC interlayer on the electrochemical behavior of the LNF//LNO//GDC//TZ3Y half-cell, samples with a GDC interlayer sintered from  $1200^\circ\text{C}$  up to  $1450^\circ\text{C}$ , for 3 h, in air, were prepared. A porous layer of LNO was deposited afterward, and sintered at  $1200^\circ\text{C}$  during 1h for all the samples, to keep the same ALS model parameters (porosity, specific surface area, etc. . .) than the ones previously calculated. Among the LNF//LNO//GDC//TZ3Y samples, delamination of the LNO electrode was observed for the samples with GDC sintered at  $1200^\circ\text{C}$  or  $1250^\circ\text{C}$ . Above  $1250^\circ\text{C}$ , good adhesion of the LNO electrodes on the GDC layer was obtained.

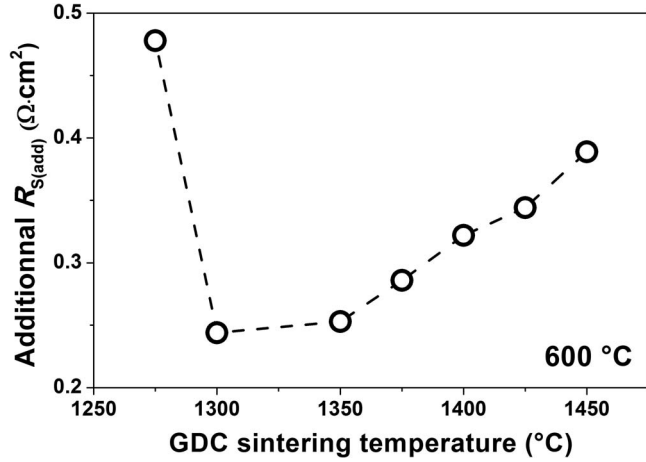


**Figure 9.** Thermal dependence of the additional series resistance related to the GDC/TZ3Y and/or LNO//GDC interfaces, measured at 600°C.

The properties of the samples were measured by EIS from 500°C up to 800°C. The series resistance  $R_S$  of the half-cells was varied with the GDC sintering temperature. Considering that the contribution of the electronic conduction of LNO and LNF to the series resistance is negligible, it was assumed that these variations in the series resistance are due to interdiffusion processes at the TZ3Y//GDC and/or GDC//LNO interfaces. To quantify these variations, subsequently named additional  $R_{S(\text{add})}$ , the contribution of the dense TZ3Y electrolyte ( $R_{S(\text{elect})}$ ) to the raw total  $R_S$  was subtracted;  $R_{S(\text{elect})}$  was calculated from the theoretical ionic conductivity of the TZ3Y electrolyte, and double-checked by measuring a reference Pt//TZ3Y//Pt half-cell by EIS (not reported). The additional  $R_{S(\text{add})}$  values calculated at 600°C are shown in Fig. 9.

The high additional  $R_{S(\text{add})}$  value obtained when GDC is sintered at 1275°C ( $R_{S(\text{add})} = 0.48 \Omega \cdot \text{cm}^2$ ) supports that GDC is not enough sintered to prevent detrimental diffusion process at the LNO//GDC interface, which results in delamination of the LNO electrode for GDC sintered at 1200°C or 1250°C. The smallest additional series resistance,  $R_{S(\text{add})} \approx 0.25 \Omega \cdot \text{cm}^2$ , was obtained for GDC sintered at 1300°C or 1350°C.

For higher sintering temperatures, the progressive increase of the  $R_S$  value likely results from the cation interdiffusion at the GDC/TZ3Y interface, as confirmed by X-ray diffraction analysis of this interface (see discussion part). Finally, the best compromise to avoid excessive interdiffusion at these interfaces would be to sinter the GDC interlayer between 1300°C and 1350°C.

Then, the polarization resistance related to the oxygen electrode reaction of the different samples was carefully examined. The Nyquist and Bode plots of the LNF//LNO//GDC//TZ3Y half-cells with GDC sintered at various temperatures are reported in Fig. 10. Whatever the samples, a Gerischer impedance is observed, the apex frequency of these impedances being quite similar,  $f \approx 2 \cdot 10^1$  Hz (Fig. 10b). However, the value of the chemical resistance related to the Gerischer impedance depends on the GDC sintering temperature: these values are reported in Table I.

The chemical resistance related to the Gerischer impedance gradually decreases with the GDC sintering temperature, down to  $R_{\text{chem}} = 0.61 \Omega \cdot \text{cm}^2$  for GDC sintered at 1400°C. Above 1400°C, the chemical resistance gradually increases. These results clearly show that

**Table I. Chemical resistance  $R_{\text{chem}}$  related to the Gerischer impedance as a function of the GDC sintering temperature.**

	GDC sintering temperature (°C)							
	1200	1275	1300	1350	1375	1400	1425	1450
$R_{\text{chem}} (\Omega \cdot \text{cm}^2)$	177.1	1.20	0.85	0.77	0.72	0.61	0.72	0.91

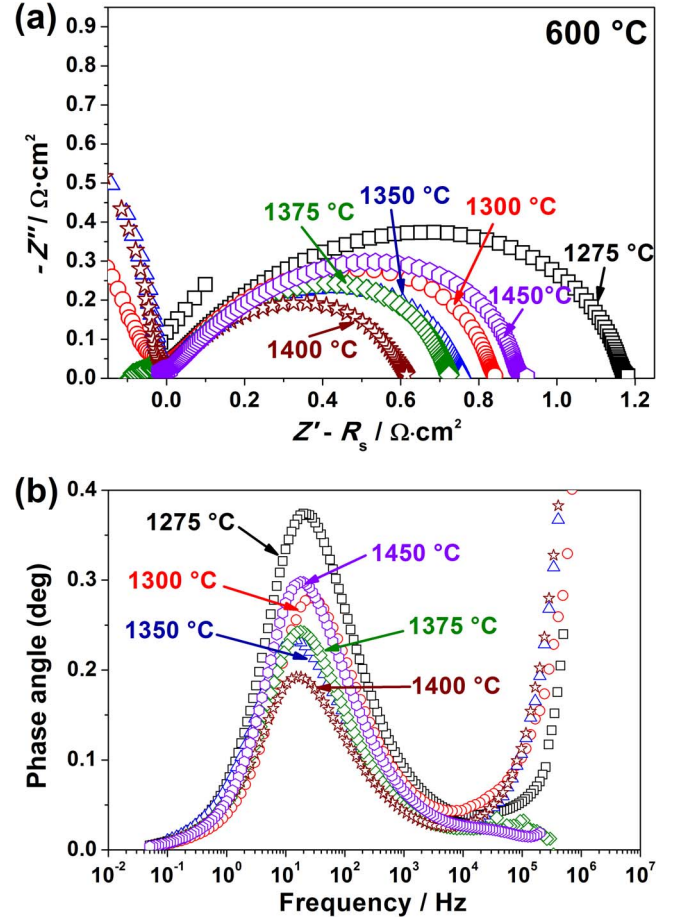


**Figure 10.** Influence of the GDC interlayer sintering temperature on the electrochemical performances of the LNF//LNO//GDC//TZ3Y half-cells at 600°C: (a) Nyquist plots, (b) Bode plots, for various GDC sintering temperatures.

the Gerischer impedance, which is usually only related to the oxygen electrode reaction in the LNO electrode, may depends on the GDC interlayer as well.

The ALS model was then applied to every samples, using the microstructural parameters previously defined for the LNO electrode.

The LNO surface exchange rate and ionic conductivity were calculated, at 600°C, for all the samples; the variations of  $\mathfrak{R}_0$  and  $\sigma_{i(\text{LNO})}$  vs. the GDC sintering temperature are shown in Figs. 11a and 11b.

In addition, the  $\mathfrak{R}_0$  and  $\sigma_{i(\text{LNO})}$  values are plotted in Figs. 12a and 12b, as a function of temperature for three samples with GDC sintered at 1275°C, 1400°C or 1450°C.

Results from Fig. 11a and Fig. 12a clearly show that the surface exchange rate is independent of the GDC sintering temperature, even for the sample with GDC sintered at 1200°C, for which delamination at the LNO//GDC interface was observed after the EIS experiments.

On the contrary, the ionic conductivity (Fig. 11b and Fig. 12b) is clearly dependent on the GDC sintering temperature. It is noteworthy that for the sample with GDC sintered at 1400°C (star plot), the  $\mathfrak{R}_0$  and  $\sigma_{i(\text{LNO})}$  calculated from the ALS model are in good agreement with the  $\mathfrak{R}_0$  and  $\sigma_{i(\text{LNO})}$  values obtained from the literature data (Fig. 12). It seems that in these conditions, the LNO//GDC interface does not limit the oxide solid state diffusion from LNO toward the GDC interlayer (and *vice-versa*).

Another interesting point is that, with a LNO particle size diameter  $\varnothing \approx 0.55 \mu\text{m}$  as prepared in this study, it seems impossible to get values of the chemical resistance  $R_{\text{chem}}$  lower than  $\approx 0.61 \Omega \cdot \text{cm}^2$  at 600°C, which is close from the value predicted by the ALS model ( $0.595 \Omega \cdot \text{cm}^2$ ). In the future, it would be interesting to study the

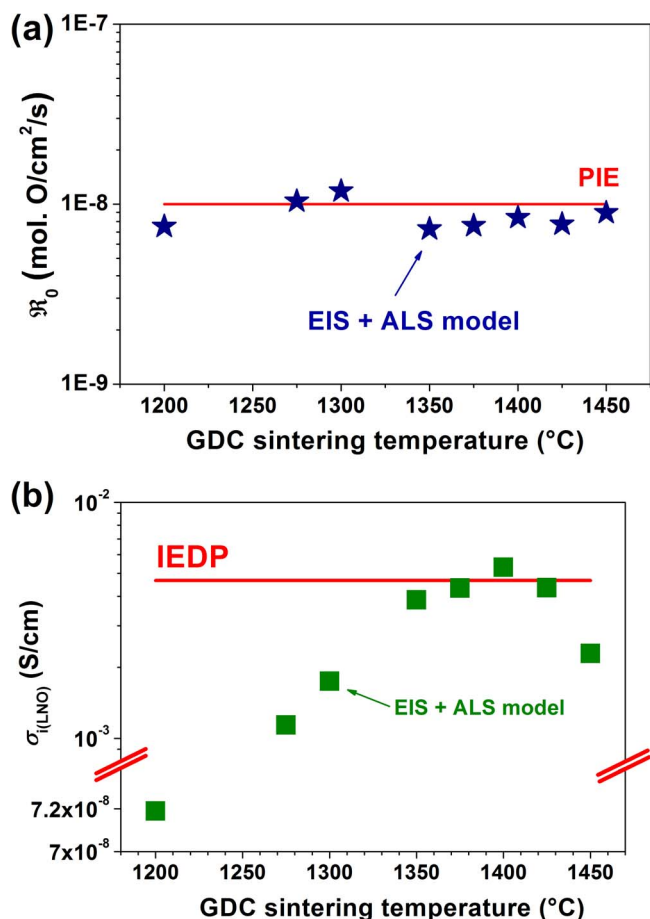


**Figure 11.** (a) Surface exchange rate and (b) ionic conductivity calculated using the ALS model at 600°C for LNF//LNO//GDC//TZ3Y half-cells as a function of the GDC sintering temperature.

influence of the particle size diameter of LNO on this chemical resistance, i.e. to increase  $S_A$ .

Furthermore, the optimal  $R_{chem}$  value obtained when GDC inter-layer is sintered at 1400°C leads to an additional series resistance  $R_{s(add)} \approx 0.32 \Omega \cdot \text{cm}^2$  at 600°C (as shown in Fig. 9), which should be taken into account when considering the electrochemical performances of the LNO//GDC//TZ3Y designed cell.

The main conclusion of this study is that the Gerischer impedance usually assigned to the LNO electrode only is actually dependent on the LNO//GDC interface. A possible explanation for this behavior is given in the following discussion.

### Discussion

As stated earlier, interdiffusion processes have been observed in the literature between LNO and GDC, leading to the formation of lanthanum doped GDC and  $\text{La}_3\text{Ni}_2\text{O}_7$  at their interface for  $T > 1000^\circ\text{C}$ .<sup>10,32</sup> To confirm this point, the LNO electrode was removed by acid leaching: XRD measurements were carried out on the top surface of the half-cells, in order to characterize the GDC layer and the GDC//TZ3Y interface. Results are shown in Fig. 13. The peak at  $2\theta_{\text{Cu}} \approx 28.3^\circ$  confirms the formation of La doped GDC.<sup>34,35</sup> In addition, cations interdiffusion at the GDC//TZ3Y interface is revealed by the progressive shift of the GDC peak from  $2\theta_{\text{Cu}} \approx 28.8^\circ$  to higher angles<sup>35</sup> and the apparition of a small shoulder at the base of the TZ3Y peak at  $2\theta_{\text{Cu}} \approx 30.3^\circ$ , when the GDC sintering temperature is increased.

Based on these observations, the oxygen electrode reaction occurring for GDC sintered at 1300°C or 1400°C, 3h, and LNO sintered at

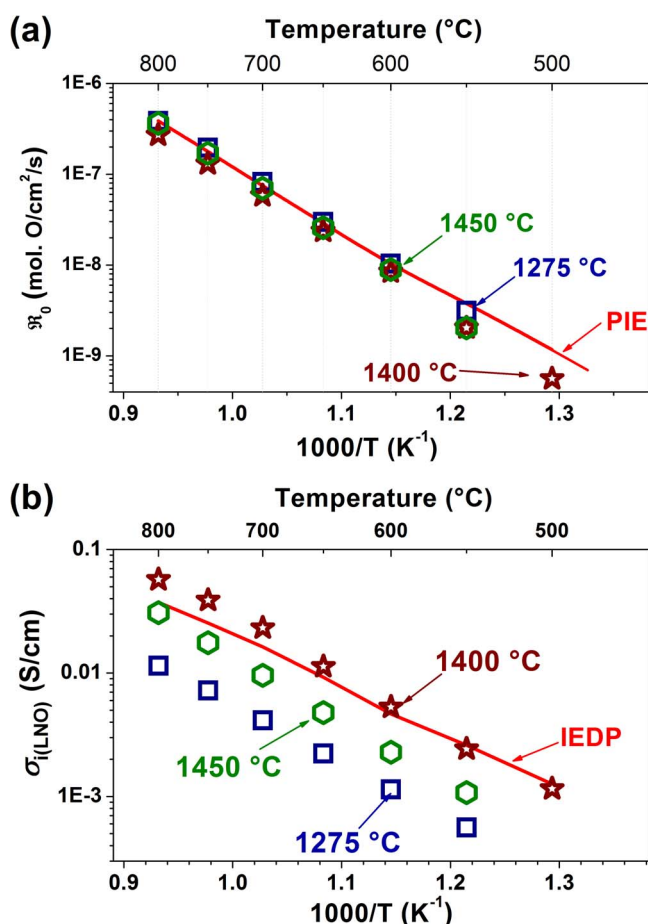


**Figure 12.** Thermal dependence of (a) the surface exchange rate and (b) the ionic conductivity calculated using the ALS model for LNF//LNO//GDC//TZ3Y half-cells, with GDC sintered at various temperatures.

1200°C, 1h, is schematically represented in Fig. 14a. Using Eq. 8 and EIS data, the calculated diffusion length at 550°C is around 4.5  $\mu\text{m}$  for GDC sintered at 1300°C, while it increases up to 10  $\mu\text{m}$  for GDC sintered at 1400°C. This difference comes from the efficiency of the ionic diffusion in the material, which is discussed below.

Assuming that GDC doped with La and/or Zr is not electronic conducting, hence, the electrical double layer takes place at the interface between the La deficient LNO phase, and the doped GDC phase (Fig. 14b). The OER occurs mostly at the LNO grains (Fig. 14a), and to a much lesser extent at the La deficient LNO phase (gray in Fig. 14b). Then, the oxygen insertion is mostly achieved by the LNO grains, as illustrated in Fig. 14a, which explains why the  $\mathfrak{R}_0$  parameter is independent of the GDC sintering temperature.

The overall ionic conductivity of the electrode  $\sigma_i$  that should be considered for the ALS model is in the best case, the ionic conductivity of the LNO grains  $\sigma_{i(LNO)}$ . This occurs when the effective ionic conductivities of all the phases concerned with the  $\text{O}^{2-}$  diffusion path, from the LNO layer to the TZ3Y electrolyte, are larger than or equal to the effective ionic conductivity of the LNO phase. Compared to the intrinsic ionic conductivity, the effective ionic conductivity takes into account the porosity and tortuosity of each phase.

It is assumed that a dense TZ3Y membrane, a quasi-dense GDC layer as well as the La deficient phase that was reported by various authors<sup>10,31</sup> to be  $\text{La}_3\text{Ni}_2\text{O}_{7-8}$ , meet this requirement. Indeed, comparison of porous  $\text{La}_3\text{Ni}_2\text{O}_{7-8}$  and LNO electrodes deposited on a LSGM electrolyte showed that the lowest polarization resistance was obtained for  $\text{La}_3\text{Ni}_2\text{O}_{6.95}$ .<sup>36</sup>

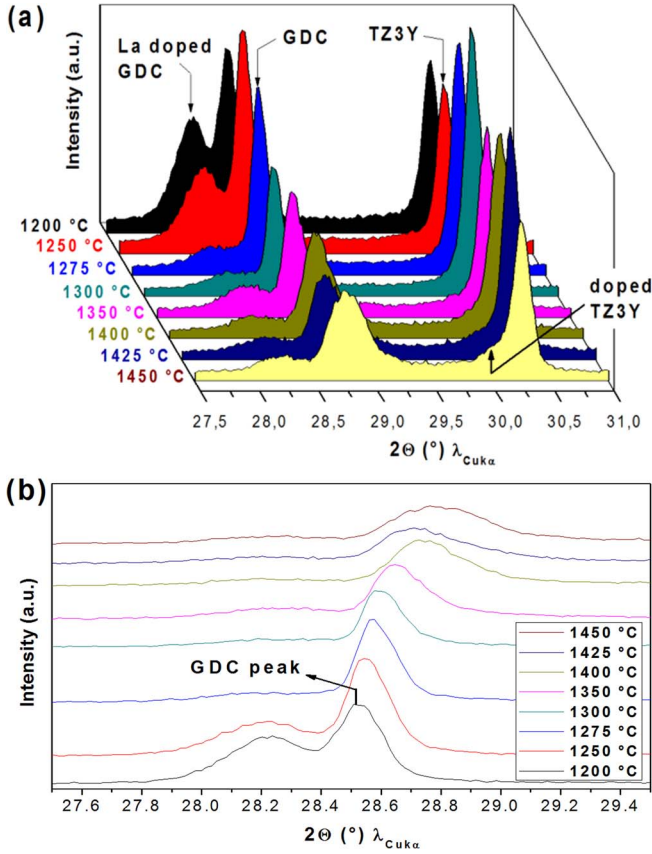


**Figure 13.** X-ray diffractograms of the top surface of GDC/TZ3Y half-cells, after removal of the LNO electrode. GDC sintered from 1200°C up to 1450°C. LNO sintered at 1200°C. (a) Wide view; (b) focus on the GDC peak shift caused by the sintering temperature.

However, it has been reported that the ionic conductivity at 800°C of a La doped ceria was  $\sigma_{i(LDC)} \approx 1.02 \cdot 10^{-5} \text{ S.cm}^{-1}$ , half the value of  $\sigma_{i(GDC)} \approx 2.08 \cdot 10^{-5} \text{ S.cm}^{-1}$ .<sup>37</sup> It is then likely that the progressive diffusions of La and/or Zr into GDC decrease its ionic conductivity, as already observed in Fig. 9. Yet it is difficult to assess at which temperature the effective ionic conductivity of the GDC, doped with La and/or Zr, will be lower than  $\sigma_{i(LNO)}^{eff}$ . Based on Table I, it likely occurs when the sintering temperature of GDC is higher than 1400°C, since the chemical resistance increases beyond this temperature.

Finally, it is proposed that the decrease of the chemical resistance, when the GDC sintering temperature is increased from 1275°C up to 1400°C, is related to the quality of the interface between the La deficient phase and the La and/or Zr doped GDC phase, where the electrical double layer takes place (Fig. 14b). This can be seen as a “bottleneck” for the oxide transfer ions from the “electrode part” toward the “electrolyte part”. If the concerned area is too narrow, i.e. the effective ionic conductivity of the interface is lower than the effective ionic conductivity of LNO, the electrochemical performances of the electrode may drastically decrease. This issue arises when the sintering of the LNO grains with the GDC grains is not achieved. In the worst scenario, i.e. when delamination of the electrode occurs, as for instance for GDC sintered at 1200°C / 1250°C, the effective ionic conductivity of the electrode  $\sigma_i$  drops from  $\approx 4 \cdot 10^{-3} \text{ S/cm}$  down to  $8 \cdot 10^{-8} \text{ S/cm}$  (Fig. 11b). In this study, the adherence of the LNO and GDC grains seems to be mostly dependent on the initial microstructure of the GDC interlayer (doped or not), on top of which the LNO electrode is sintered. This microstructure changes with the densification of the GDC interlayer, i.e. with its sintering temperature, as already shown in Fig. 14a.

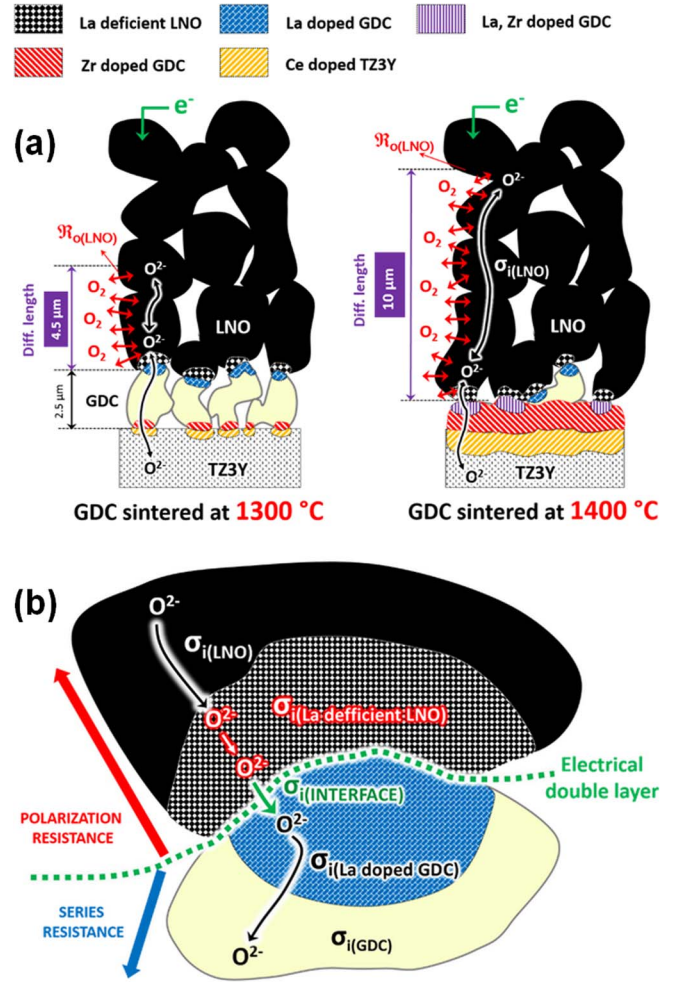


**Figure 14.** Interdiffusion process at the LNO/GDC interface affecting the solid-state diffusion of the oxide anions through the half-cell. Illustration of the diffusion length calculated at 550°C for GDC sintered either at 1300°C or 1400°C, and LNO sintered at 1200°C. (a) Global view (b) zoom at the LNO/GDC interface for GDC sintered at 1300°C.

The main conclusions of this part are summed up in Fig. 15, where the evolution of the additional series resistance (previously reported in Fig. 9) and of the chemical resistance with the GDC sintering temperature are compared.

Results of Fig. 15 points out that the lowest chemical resistance is not necessarily correlated with the lowest series resistance.

Theoretically, the Gerischer impedance related to the ALS model should only be used when the oxygen exchange and the oxide diffusion in LNO contribute to the OER. However, this study shows that when the ionic diffusion in LNO is hindered, due to the presence of detrimental La doped GDC at its interface for instance, the Gerischer impedance still accurately fit the data. In that case, the ionic conductivity of LNO,  $\sigma_{i(MIEC)}$  in Eq. 3, must be replaced by an apparent ionic conductivity  $\sigma_{i(app)}$ , which takes into account issues in the  $O^{2-}$  diffusion path occurring in the whole half cell:

$$R_{chem} = \sqrt{\frac{RT}{2F^2}} \times \frac{\tau}{(1 - \varepsilon) \cdot S_A \cdot \mathfrak{R}_{O(MIEC)} \cdot \sigma_{i(app)}} \quad [16]$$

If the calculated  $\sigma_{i(app)}$  exhibits a lower value than the expected  $\sigma_{i(LNO)}$ , it will indicate that the LNO/GDC and/or GDC/TZ3Y interfacial areas have poor ionic conductivities. The authors believe that the main drawbacks to the electrochemical performances of SOFC electrodes are, besides the issues of current collecting, their reactivity with

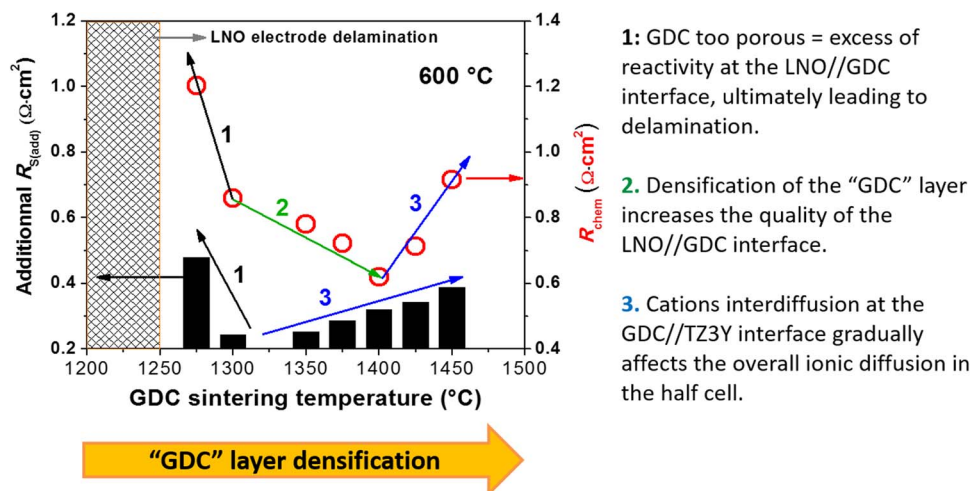


**Figure 15.** Variation of the additional series resistance and chemical resistance of a LNO//GDC//TZ3Y half-cell, as a function of the GDC sintering temperature, at 600°C. LNO sintered at 1200°C for 1 h.

their respective interface materials. These issues must be solved first, before considering optimizing the shaping of the electrode grains.

### Conclusions

This study was focused on modeling the impedance data measured by electrochemical impedance spectroscopy on a MIEC  $\text{La}_2\text{NiO}_{4+\delta}$  (LNO) porous electrode deposited on a GDC//TZ3Y half-cell, using the Adler-Lane-Steele (ALS) model. The sintering of the LNO electrode was fixed to 1200°C, while the sintering temperature of the GDC interlayer was varied from 1200°C up to 1450°C. For all the samples, the oxygen electrode reaction (OER) occurring at the LNO electrode was measured by EIS as Gerischer impedances, for temperatures ranging from 500°C up to 800°C. Surprisingly, the polarization resistance of these Gerischer impedances was shown to vary with the sintering temperature of the barrier layer, GDC.

Theoretically, the ALS model states that in the limit where the resistance related to the OER in the half-cell only depends on the diffusion of oxygen in the electrode, and on the exchange of  $\text{O}_2$  at the electrode/gas interface, a Gerischer impedance is obtained. In this study, we showed that when the ionic diffusion in the LNO electrode is hindered due to interfacial issues with its electrolyte, the Gerischer impedance predicted by the ALS model can still be used to accurately model the data. In that case, it is necessary to consider an “apparent” ionic conductivity  $\sigma_{i(\text{app})}$  in the expression of the Gerischer, instead of the ionic conductivity of LNO  $\sigma_{i(\text{LNO})}$ . This apparent ionic conductivity outlines potential “bottleneck” in the ionic diffusion pathway from the electrode toward the electrolyte part of the half-cell.

For GDC sintered at 1400°C, 3h, and LNO sintered at 1200°C, 1h, it has been calculated that  $\sigma_{i(\text{app})} \approx \sigma_{i(\text{LNO})}$ . In that case, the LNO//GDC interface does not limit the  $\text{O}_2$  solid-state diffusion in the half cell, which gives the best electrode electrochemical performance that can be expected for a LNO electrode with a particle diameter  $\phi \approx 0.55 \mu\text{m}$ , which is  $R_{\text{chem}} \approx 0.61 \Omega \cdot \text{cm}^2$  at 600°C. However, due to cations interdiffusion at the GDC//TZ3Y interface at 1400°C, which likely lead to the formation of phase(s) with an effective ionic diffusion lower than those of GDC and TZ3Y, additional series resistance  $R_{s(\text{add})} \approx 0.32 \Omega \cdot \text{cm}^2$  appears, as compared to the series resistance expected for an ideal GDC//TZ3Y architecture. Other candidates than GDC as interlayer between TZ3Y and LNO should be considered, in order to fix that issue.

### Acknowledgment

The research leading to these results has received funding from the European Union’s Seventh Framework Programme (FP7/2007-2013)

**1:** GDC too porous = excess of reactivity at the LNO//GDC interface, ultimately leading to delamination.

**2:** Densification of the “GDC” layer increases the quality of the LNO//GDC interface.

**3:** Cations interdiffusion at the GDC//TZ3Y interface gradually affects the overall ionic diffusion in the half cell.

for Fuel Cells and Hydrogen Joint Technology Initiative under grant agreement n° [256768] 10. The authors gratefully acknowledge the European Community for supporting this work through the RAMSES project.

### References

- J. C. Grenier, J. M. Bassat, and F. Mauvy, in *Funct. mat. sustain. energy applications*, J. A. Kilner, S. J. Skinner, S. J. C. Irvine, and P. P. Edwards, Editors, p. 402, Woodhead Publishing (2012).
- C. Laberty, F. Zhao, K. E. Swider-Lyons, and A. V. Virkar, *Electrochem. Solid State Lett.*, **10**, B170 (2007).
- C. Ferchaud, J. C. Grenier, Y. Zhang-Steenwinkel, M. M. A. van Tuel, F. P. F. van Berkel, and J. M. Bassat, *J. Power Sources*, **196**, 1872 (2011).
- J. M. Bassat, P. Odier, A. Villesuzanne, C. Marin, and M. Pouchard, *Solid State Ionics*, **167**, 341 (2004).
- M. Burriel, J. Santiso, M. D. Rossell, G. Van Tendeloo, A. Figueras, and G. Garcia, *J. Phys. Chem. C*, **112**, 10982 (2008).
- A. Flura, S. Dru, C. Nicollet, V. Vibhu, S. Fourcade, E. Lebraud, A. Rougier, J.-M. Bassat, and J.-C. Grenier, *J. Solid State Chem.*, **228**, 189 (2015).
- N. Hildenbrand, P. Nammensma, D. H. A. Blank, H. J. M. Bouwmeester, and B. A. Boukamp, *J. Power Sources*, **238**, 442 (2013).
- S. B. Adler, J. A. Lane, and B. C. H. Steele, *J. Electrochem. Soc.*, **143**, 3554 (1996).
- Y. Takeda, M. Nishijima, N. Imanishi, R. Kanno, and O. Yamamoto, *J. Solid State Chem.*, **96**, 72 (1992).
- A. M. Hernández, L. Mogni, and A. Caneiro, *Internat. J. Hydrogen Energy*, **35**, 6031 (2010).
- C. Nicollet, A. Flura, V. Vibhu, A. Rougier, J. M. Bassat, and J. C. Grenier, *J. Power Sources*, **294**, 473 (2015).
- T. Roisnel and J. Rodriguez-Carvajal, in *Epdic 7: Eur. Powder Diffr., Pts 1 and 2*, R. Delhez and E. J. Mittemeijer, Editors, p. 118 (2001).
- B. Zeimet, Comprehensive analysis of experiments linked to EIS, CANEELS, in (2014).
- B. A. Boukamp, *Solid State Ionics*, **62**, 131 (1993).
- S. B. Adler, *Solid State Ionics*, **135**, 603 (2000).
- S. B. Adler, *Chem. Rev.*, **104**, 4791 (2004).
- H. Gerischer, *Z. Phys. Chem.*, **198**, 286 (1951).
- M. Sluyters-Rehbach and J. H. Sluyters, in *Compr. Treatise of Electrochem.*, E. Yeager, Editor, p. 274, New York (1984).
- B. A. Boukamp and H. J. M. Bouwmeester, *Solid State Ionics*, **157**, 29 (2003).
- J. Fleig, *Annu. Rev. Mat. Res.*, **33**, 361 (2003).
- F. Mauvy, C. Lalanne, J.-M. Bassat, J.-C. Grenier, H. Zhao, L. Huo, and P. Stevens, *J. Electrochem. Soc.*, **153**, 1547 (2006).
- W. G. Bessler, *J. Electrochem. Soc.*, **153**, A1492 (2006).
- A. Flura, C. Nicollet, S. Fourcade, V. Vibhu, A. Rougier, J. M. Bassat, and J. C. Grenier, *Electrochimica Acta*, **174**, 1030 (2015).
- M. Urquidi-Macdonald, S. Real, and D. D. Macdonald, *Electrochimica Acta*, **35**, 1559 (1990).
- J. B. Jorcin, M. E. Orazem, N. Pebere, and B. Tribollet, *Electrochimica Acta*, **51**, 1473 (2006).
- E. Y. Pikalova, N. M. Bogdanovich, A. A. Kolchugin, D. A. Osinkin, and D. I. Bronin, *Proc. Engin.*, **98**, 105 (2014).
- F. Mauvy, J. M. Bassat, E. Boehm, P. Dordor, J. C. Grenier, and J. P. Loup, *J. Eur. Ceram. Soc.*, **24**, 1265 (2004).
- Y. Lu, C. Kreller, and S. B. Adler, *J. Electrochem. Soc.*, **156**, B513 (2009).
- Y.-c. K. Chen-Wiegart, R. DeMike, C. Erdonmez, K. Thornton, S. A. Barnett, and J. Wang, *J. Power Sources*, **249**, 349 (2014).

30. H. J. M. Bouwmeester, C. Song, J. Zhu, J. Yi, and M. v. S. Annaland and B. A. Boukamp, *Phys. Chem. Chem. Phys.*, **11**, 9640 (2009).
31. G. Amow, P. S. Whitfield, I. J. Davidson, R. P. Hammond, C. N. Munnings, and S. J. Skinner, *Ceram. Internatl.*, **30**, 1635 (2004).
32. R. Sayers, J. Liu, B. Rustumji, and S. J. Skinner, *Fuel Cells*, **8**, 338 (2008).
33. A. Montenegro-Hernández, A. Soldati, L. Mogni, H. Troiani, A. Schreiber, F. Soldera, and A. Caneiro, *J. Power Sources*, **265**, 6 (2014).
34. N. Jaiswal, S. Upadhyay, D. Kumar, and O. Parkash, *J. Power Sources*, **222**, 230 (2013).
35. L. Katta, P. Sudarsanam, G. Thrimurthulu, and B. M. Reddy, *Appl. Catal. B: Environ.*, **101**, 101 (2010).
36. G. Amow, I. J. Davidson, and S. J. Skinner, *Solid State Ionics*, **177**, 1205 (2006).
37. M. Mogensen, N. M. Sammes, and G. A. Tompsett, *Solid State Ionics*, **129**, 63 (2000).